

Stress–softening and recovery of elastomers

Aleksey D. Drozdov¹ and Al Dorfmann²

¹ *Institute for Industrial Mathematics, 4 Hanachtom Street*

84311 Beersheba, Israel

² *Institute of Structural Engineering, 82 Peter Jordan Street*

1190 Vienna, Austria

Abstract

A constitutive model is developed for the mechanical response of elastomers at finite strains. A polymer is treated as a network of linear chains linked by permanent (chemical crosslinks) and temporary (entanglements and van der Waals forces) junctions. Temporary junctions are assumed to be in two states: loose (passive) when they impose only topological constraints on available configurations of chains, and tight (active) when their effect is tantamount to that for crosslinks. Stretching of a specimen implies that some loose junctions become active, which decreases the average length of a chain.

A long chain is treated as an ensemble of inextensible strands connected in sequel. Two neighboring strands are bridged by a bond which may be in two conformations: flexed (trans) and extended (cis). A bond in the flexed conformation is modeled as a linear elastic solid, whereas the mechanical energy of a bond in the extended conformation (two rigid rods directed along a straight line) is disregarded. For a virgin specimen, all bonds are in the flexed conformation. Under loading some bonds are transformed from flexed to extended conformation.

Stress–strain relations for a rubbery polymer and kinetic equations for the trans–cis transition are derived using the laws of thermodynamics. Governing equations

are determined by 5 adjustable parameters which are found by fitting experimental data in uniaxial tensile tests on natural rubber vulcanizates with various amounts of crosslinks. Fair agreement is demonstrated between results of numerical simulation and observations with the elongation ratio up to $k = 8$. We analyze the effects of cyclic loading, thermal annealing and recovery by swelling on the material constants.

Key-words: Elastomers, Stress-softening, Recovery, Rigid-rod chains, Temporary networks

1. Introduction

This study is concerned with modeling stress-softening and subsequent recovery (by annealing at an elevated temperature and by swelling) of elastomers. Stress-strain relations for unfilled and particle reinforced rubbery polymers have been the focus of attention in the past four decades. This may be explained by numerous applications of rubbery-like materials in industry (vehicle tires, seals, shock absorbers, flexible joints, etc.), as well as by some peculiarities in their mechanical behavior whose physical mechanisms are not quite clear. A renewal of the interest to the mechanical response of elastomers observed in the past decade, see Refs.^{1–15}, is associated with the development of constitutive equations that (i) account for the molecular structure of polymers at the micro-level and (ii) describe some features of their response induced by time-dependent changes in the internal structure (viscoplasticity, damage, micro-fracture, etc.).

Among these peculiarities, one of the most important for applications is the Mullins effect¹⁶. This phenomenon is evidenced in tensile^{17–20}, compressive⁹ and shear²¹ tests as a noticeable difference between the stress-strain curve for a virgin specimen and that for the material reloaded after retraction. A conventional standpoint is that cyclic pre-stretching with 3 to 6 cycles and the maximum elongation ratio of about $k = 2$ makes the response of an elastomer repeatable⁹. However, the number of cycles, as well as their amplitude and frequency are chosen by the trial-and-error method and substantially depend on what the

repeatability of a stress–strain diagram means for the experimentalist.

Although the physical mechanism of the Mullins effect in unfilled elastomers remains hitherto obscure, it is traditionally associated with material damage^{1,11,15}, non-affinity of deformation for a polymeric network^{10,21}, viscous drag exerted on the network chains by their environment²² and mechanically-induced crystallization of rubbery polymers²⁰. These reasons may, however, be questioned, because observations reveal that with an increase in strains above the maximal level reached at pre-stretching, the stress–strain curve returns to that for a virgin sample.

The present study aims to explain stress-softening of elastomers under cyclic loading by an increase in the average size of globules formed by polymeric chains (uncoiling of macromolecules). For this purpose, we develop a phenomenological model for the stress–strain response of rubbery polymers and determine its parameters by fitting experimental data in uniaxial tensile tests for virgin, pre-stretched and recovered specimens.

An elastomer is taken as a network of linear macromolecules bridged by permanent (chemical crosslinks) and temporary (physical crosslinks, entanglements and van der Waals forces) junctions. For the sake of simplicity, it is presumed that junctions move affinely with the bulk material. The novelty of our approach is that the number of junctions is not fixed, but assumed to alter under loading. To explain this phenomenon, we ascribe two possible states to an entanglement: loose (passive) and tight (active). An entanglement in the loose state does not create a junction, but imposes only topological constraints on the number of available configurations for a chain. On the contrary, an entanglement in the tight state is thought of as the same junction as that formed by a chemical crosslink. The transition of an entanglement from its passive state to the active state (tightening of entanglements) is supposed to be driven by mechanical factors. Introducing a simple kinetic equation for the rate of this transition, we study the response of a temporary network with a time-varying number of junctions.

A chain that connects two neighboring junctions is modeled as a sequence of strands (statistically independent segments) bridged by bonds²³. With reference to the Kratky–

Porod concept²⁴, strands are taken as inextensible (rigid) rods, whereas the mechanical energy of a chain is determined as the sum of strain energies for bonds. It is postulated that a bond may be in two stable conformations: flexed (trans) and extended (cis). A bond in the flexed conformation is thought of as a linear elastic solid, whereas the mechanical energy of a bond in the extended conformation vanishes. Constitutive equations for an elastomer and the kinetic equations for the transition of bonds from their flexed to extended conformations are derived by using the laws of thermodynamics. The development of stress–strain relations is based on the hypothesis that the characteristic time for changes in the concentration of active entanglements substantially exceeds that for mechanical deformation.

The paper is organized as follows. Deformation of a chain is discussed in Section 2. The mechanical energy of a temporary network is determined in Section 3. Stress–strain relations are developed in Section 4 using the laws of thermodynamics. Kinetic equations for transition of entanglements from their loose to tight state are introduced in Section 5. Uniaxial extension of a specimen is studied in Section 6. Results of numerical simulation are compared with experimental data for natural rubber vulcanizates in Section 7. Section 8 deals with the effects of cyclic stretching and recovery on experimental constants. Some concluding remarks are formulated in Section 9.

2. Deformation of a long chain

An elastomer is modeled as an ensemble of linear macromolecules bridged by crosslinks, entanglements and van der Waals forces. Active links between macromolecules are thought of as junctions (permanent in the case of chemical crosslinks and temporary for entanglements and van der Waals forces). A sequence of mers (belonging to a polymeric molecule) between two subsequent junctions is associated with a chain. Chains are divided into strands (statistically independent segments) bridged by bonds. In accord with the Kratky–Porod model, a chain is treated as an aggregate consisting of $N + 1$ identical inextensible strands linked in sequel. The average number of bonds in a chain change under stretching of a specimen

because of slippage of entanglements with respect to chains and transition of entanglements from their loose to the tight state. This implies that N is taken as a function of time, $N = N(t)$.

We adopt a zigzag model²⁵ and assume that a bond bridging two neighboring strands is characterized by one of the two stable conformations: flexed and extended. In the stress-free state the angle between two strands linked by a bond in the flexed conformation equals $\theta \in (0, \pi)$ (the same for all bonds) and that for a bond in the extended conformation equals π (see a sketch depicted in Figure 1 of Ref.³¹). In thermal equilibrium before deformation all bonds are in the flexed conformation. Mechanical loading activates chains, which implies that conformations of some bonds alter. The numbers of bonds in flexed and extended conformations, $N_f(t)$ and $N_e(t)$, obey the balance law

$$N_f(t) + N_e(t) = N(t).$$

Introducing the average concentration of bonds in the extended conformation, $n = n(t)$, we obtain

$$N_f(t) = N(t)[1 - n(t)], \quad N_e(t) = N(t)n(t). \quad (1)$$

In a deformed state the angle between strands linked by a bond in the flexed conformation changes, whereas for a bond in the extended conformation (modeled as two rigid rods directed along a straight line) this angle remains unaltered. The strain, e , from the stress-free state of a chain to its deformed state equals the sum of strains for bonds in the flexed conformation,

$$e = N_f e_f.$$

This equality together with Eq. (1) implies that

$$e_f = \frac{e}{N(1 - n)}. \quad (2)$$

Bonds in the flexed conformation are modeled as linear elastic solids with the mechanical energy

$$\frac{1}{2}\mu e_f^2,$$

whereas the strain energy of bonds in the extended conformation vanishes. The mechanical energy of a chain, w , equals the sum of the mechanical energies for individual bonds. It follows from Eqs. (1) and (2) that

$$w(e) = \frac{\mu e^2}{2N(1-n)}. \quad (3)$$

To express the strain in a chain, e , in terms of the macro-strain tensor for a network, $\hat{\epsilon}$, we consider a chain connecting neighboring junctions $A_1(t)$ and $A_2(t)$. Let $\bar{r}_{01}(t)$ and $\bar{r}_{02}(t)$ be radius vectors of these points in the stress-free state and $\bar{r}_1(t)$ and $\bar{r}_2(t)$ their radius vectors in the deformed state at time $t \geq 0$. The end-to-end length of the chain reads $\delta_0(t)$ in the stress-free state and $\delta(t)$ in the deformed state. Introducing the guiding vector in the stress-free state, \bar{l} , (the unit vector directed along the end-to-end vector for the chain), we obtain

$$\bar{r}_{02}(t) - \bar{r}_{01}(t) = \delta_0(t)\bar{l}.$$

In the deformed state, the junctions occupy points with the radius vectors

$$\bar{r}_1(t) = \bar{r}_{01}(t) + \bar{u}(t, \bar{r}_{01}(t)), \quad \bar{r}_2(t) = \bar{r}_{02}(t) + \bar{u}(t, \bar{r}_{02}(t)),$$

where $\bar{u}(t, \bar{r})$ is the displacement vector at point \bar{r} for transition from the stress-free state to the deformed state at time t . The end-to-end vector for the chain in the deformed state is given by

$$\bar{R}(t) = \bar{r}_2(t) - \bar{r}_1(t) = \delta_0(t)\bar{l} + [\bar{u}(t, \bar{r}_{01}(t) + \delta_0(t)\bar{l}) - \bar{u}(t, \bar{r}_{01}(t))].$$

Neglecting terms beyond the first order of smallness compared to $\delta_0(t)$, we find that

$$\bar{R}(t) = \delta_0(t)\bar{l} \cdot [\hat{I} + \bar{\nabla}_0 \bar{u}(t)],$$

where $\bar{\nabla}_0$ is the gradient operator in the stress-free state, \hat{I} is the unit tensor, the dot stands for inner product and the argument \bar{r}_{01} is omitted. In terms of the radius vector in the deformed state, \bar{r} , this equality reads

$$\bar{R}(t) = \delta_0(t) \bar{l} \cdot \bar{\nabla}_0 \bar{r}(t) = \delta_0(t) [\bar{\nabla}_0 \bar{r}(t)]^\top \cdot \bar{l}, \quad (4)$$

where \top stands for transpose. The end-to-end length of the chain in the deformed state, $\delta(t)$, is given by

$$\delta^2 = \bar{R} \cdot \bar{R}.$$

This equality together with Eq. (4) yields

$$\delta^2(t, \bar{l}) = \delta_0^2(t) \bar{l} \cdot \hat{C}(t) \cdot \bar{l}, \quad (5)$$

where

$$\hat{C}(t) = \bar{\nabla}_0 \bar{r}(t) \cdot [\bar{\nabla}_0 \bar{r}(t)]^\top \quad (6)$$

is the Cauchy deformation tensor for transition from the stress-free state of the network to its deformed state at time t .

The extension ratio for the chain, $\lambda(t, \bar{l})$, is defined as the ratio of the current end-to-end length, $\delta(t, \bar{l})$, to that of the chain in its activated stress-free state, $\delta^\circ(t, \bar{l})$. The latter state is defined as a state in which the chain is unloaded, but the numbers of bonds in various conformations coincide with their current values, $N_f(t, \bar{l})$ and $N_e(t, \bar{l})$. It differs from the equilibrium stress-free state of the chain, where the number of bonds in the extended conformation vanishes. The difference between the end-to-end lengths of a chain in the activated state, $\delta^\circ(t, \bar{l})$, and in the equilibrium state, $\delta_0(t)$, determines the end-to-end elongation driven by transformation of bonds from their flexed conformation to the extended conformation. We assume that the transformation-induced end-to-end elongation is proportional to the number of bonds acquiring the extended conformation,

$$\delta^\circ(t, \bar{l}) = \delta_0(t) [1 + \eta n(t, \bar{l})], \quad (7)$$

where $\eta > 0$ characterizes an increment of the end-to-end length driven by an individual transition. The quantity η reflects the average size of a globule created by a polymeric chain: when η is small, the chain is rolled into a tight coil, whereas an increase in η is tantamount

to unfolding the coil. Because the parameter η describes the current state of a chain, it should be thought of as a function of time (strain). To simplify calculations, we treat it as a constant, but suppose that η can change from one stress-strain curve to another in cyclic tests.

It follows from Eqs. (5) and (7) that the Hencky strain for a chain, $e = \ln \lambda$, reads

$$e(t, \bar{l}) = \ln \frac{\delta(t, \bar{l})}{\delta^\circ(t, \bar{l})} = \frac{1}{2} \ln [\bar{l} \cdot \hat{C}(t) \cdot \bar{l}] - \ln [1 + \eta n(t, \bar{l})]. \quad (8)$$

Equations (3) and (8) determine the mechanical energy of a chain, w , in terms of the Cauchy deformation tensor for the network, \hat{C} .

3. Strain energy density of a network

We adopt the conventional hypothesis that the excluded-volume effect and other multi-chain effects are screened for an individual chain by surrounding macromolecules²⁶. This implies that the energy of interaction between chains is neglected (under the incompressibility condition for the network) and the mechanical energy of the network equals the sum of the strain energies for individual chains. Assuming the distribution of chains to be isotropic, we find the concentration of chains in a network (per unit mass) with guiding vector \bar{l} ,

$$X(t, \bar{l}) = \frac{\Xi(t)}{4\pi} \sin \vartheta d\vartheta d\varphi,$$

where ϑ and φ are Euler's angles which determine the position of the unit vector \bar{l} with respect to some Cartesian coordinate frame and $\Xi(t)$ is the number of chains (per unit mass) at time $t \geq 0$. To determine the strain energy of a network, we multiply the number of chains, $X(t, \bar{l})$, by their mechanical energy, w , and sum the results for various guiding vectors, \bar{l} ,

$$W(t) = \frac{\mu \Xi(t)}{8\pi N(t)} \int_0^{2\pi} d\varphi \int_0^\pi \frac{e^2(t, \vartheta, \varphi)}{1 - n(t, \vartheta, \varphi)} \sin \vartheta d\vartheta. \quad (9)$$

The quantities $N(t)$ and $\Xi(t)$ are connected by the mass conservation law

$$mN(t)\Xi(t) = 1, \quad (10)$$

where m stands for the average mass of a strand. It follows from Eqs. (9) and (10) that

$$W(t) = \frac{\mu m \Xi^2(t)}{8\pi} \int_0^{2\pi} d\varphi \int_0^\pi \frac{e^2(t, \vartheta, \varphi)}{1 - n(t, \vartheta, \varphi)} \sin \vartheta d\vartheta. \quad (11)$$

Let Ξ_* be the average concentration of chains (per unit mass) in a (hypothetical) totally disentangled network and $M(t)$ the current number of active entanglements per unit mass. Because any tight entanglement doubles the number of chains involved in the knot, the concentration of chains in the entangled network reads

$$\Xi(t) = \Xi_* + 2M(t) = \Xi_0[1 + \nu(t)], \quad (12)$$

where $\Xi_0 = \Xi_* + 2M(0)$ is the average number of chains (per unit mass) in an equilibrium network (before a test) and the dimensionless function

$$\nu(t) = 2 \frac{M(t) - M(0)}{\Xi_0} \quad (13)$$

characterizes the ratio of the number of loose entanglements that have transformed into the active state within the interval $[0, t]$ to the initial number of chains. Combining Eqs. (11) and (12), we obtain

$$W(t) = \frac{\mu m \Xi_0^2}{8\pi} [1 + \nu(t)]^2 \int_0^{2\pi} d\varphi \int_0^\pi \frac{e^2(t, \vartheta, \varphi)}{1 - n(t, \vartheta, \varphi)} \sin \vartheta d\vartheta. \quad (14)$$

The average mechanical energy per chain is given by

$$w_0(t) = \frac{W(t)}{\Xi(t)}.$$

Substitution of Eqs. (12) and (14) into this equality yields

$$w_0(t) = \frac{\mu m \Xi_0}{8\pi} [1 + \nu(t)] \int_0^{2\pi} d\varphi \int_0^\pi \frac{e^2(t, \vartheta, \varphi)}{1 - n(t, \vartheta, \varphi)} \sin \vartheta d\vartheta. \quad (15)$$

Our objective now is to calculate the derivative of the function W with respect to time. For this purpose, we suppose that the characteristic rate for transition of bonds from their flexed to extended conformation substantially exceeds that for changes in the concentration

of active (tight) entanglements. This assumption may be explained by the fact that the characteristic length of a chain (the length between neighboring entanglements) dramatically exceeds that for a strand (the length-scale associated with a bond). This implies that the function $\nu(t)$ may be treated as a constant when expression (14) is differentiated with respect to t . Bearing this hypothesis in mind, we find from Eq. (14) that

$$\begin{aligned}\frac{dW}{dt}(t) &= \frac{\mu m \Xi_0^2}{4\pi} [1 + \nu(t)]^2 \int_0^{2\pi} d\varphi \int_0^\pi \frac{e(t, \vartheta, \varphi)}{1 - n(t, \vartheta, \varphi)} \frac{\partial e}{\partial t}(t, \vartheta, \varphi) \sin \vartheta d\vartheta + J_1(t), \\ J_1(t) &= \frac{\mu m \Xi_0^2}{8\pi} [1 + \nu(t)]^2 \int_0^{2\pi} d\varphi \int_0^\pi \frac{e^2(t, \vartheta, \varphi)}{[1 - n(t, \vartheta, \varphi)]^2} \frac{\partial n}{\partial t}(t, \vartheta, \varphi) \sin \vartheta d\vartheta.\end{aligned}\quad (16)$$

It follows from Eq. (8) that

$$\frac{\partial e}{\partial t}(t, \bar{l}) = \frac{1}{2[\bar{l} \cdot \hat{C}(t) \cdot \bar{l}]} \left[\bar{l} \cdot \frac{d\hat{C}}{dt}(t) \cdot \bar{l} \right] - \frac{\eta}{1 + \eta n(t, \bar{l})} \frac{\partial n}{\partial t}(t, \bar{l}). \quad (17)$$

Differentiation of Eq. (6) with respect to time yields

$$\frac{d\hat{C}}{dt}(t) = \bar{\nabla}_0 \bar{v}(t) \cdot [\bar{\nabla}_0 \bar{r}(t)]^\top + \bar{\nabla}_0 \bar{r}(t) \cdot [\bar{\nabla}_0 \bar{v}(t)]^\top,$$

where $\bar{v}(t) = d\bar{r}(t)/dt$ is the velocity vector for the network. Taking into account that

$$\bar{\nabla}_0 \bar{v}(t) = \bar{\nabla}_0 \bar{r}(t) \cdot \bar{\nabla}(t) \bar{v}(t),$$

where $\bar{\nabla}(t)$ is the gradient operator in the deformed state at time t , we obtain

$$\frac{d\hat{C}}{dt}(t) = 2\bar{\nabla}_0 \bar{r}(t) \cdot \hat{D}(t) \cdot [\bar{\nabla}_0 \bar{r}(t)]^\top, \quad (18)$$

where

$$\hat{D}(t) = \frac{1}{2} \left[\bar{\nabla}(t) \bar{v}(t) + (\bar{\nabla}(t) \bar{v}(t))^\top \right]$$

is the rate-of-strain tensor for the network. It follows from Eq. (18) that

$$\bar{l} \cdot \frac{d\hat{C}}{dt}(t) \cdot \bar{l} = 2\bar{l} \cdot \bar{\nabla}_0 \bar{r}(t) \cdot \hat{D}(t) \cdot [\bar{\nabla}_0 \bar{r}(t)]^\top \cdot \bar{l} = 2\hat{F}(t, \bar{l}) : \hat{D}(t), \quad (19)$$

where

$$\hat{F}(t, \bar{l}) = [\bar{\nabla}_0 \bar{r}(t)]^\top \cdot (\bar{l} \otimes \bar{l}) \cdot \bar{\nabla}_0 \bar{r}(t) \quad (20)$$

is the generalized Finger tensor²⁷, the colon stands for convolution and \otimes denotes tensor product. Substitution of Eqs. (17) and (19) into Eq. (16) implies that

$$\begin{aligned} \frac{dW}{dt}(t) &= \hat{\Upsilon}(t) : \hat{D}(t) - J(t), \\ \hat{\Upsilon}(t) &= \frac{\mu m \Xi_0^2}{4\pi} [1 + \nu(t)]^2 \int_0^{2\pi} d\varphi \int_0^\pi \frac{e(t, \vartheta, \varphi)}{1 - n(t, \vartheta, \varphi)} \frac{\hat{F}(t, \vartheta, \varphi)}{\bar{l} \cdot \hat{C}(t) \cdot \bar{l}} \sin \vartheta d\vartheta, \\ J(t) &= \frac{\mu m \Xi_0^2}{8\pi} [1 + \nu(t)]^2 \int_0^{2\pi} d\varphi \int_0^\pi \frac{H(t, \vartheta, \varphi)}{[1 - n(t, \vartheta, \varphi)]^2} \frac{\partial n}{\partial t}(t, \vartheta, \varphi) \sin \vartheta d\vartheta, \\ H(t, \vartheta, \varphi) &= e(t, \vartheta, \varphi) \left\{ \frac{2\eta[1 - n(t, \vartheta, \varphi)]}{1 + \eta n(t, \vartheta, \varphi)} - e(t, \vartheta, \varphi) \right\}. \end{aligned} \quad (21)$$

4. Constitutive equations

Observations evidence that under cyclic loading with small frequency (less than 10 Hz), the temperature increment is negligible and temperature T remains close to its reference value T_0 ²⁸. This means that the effect of temperature on material parameters, as well as thermal expansion of the network may be disregarded. It is assumed that the deformation process is rather slow, which implies that at any instant $t \geq 0$ thermodynamic potentials are correctly defined. For affine deformation of an incompressible network, the Clausius–Duhem inequality reads²⁹

$$T \frac{dQ}{dt} = -S \frac{dT}{dt} - \frac{d\Psi}{dt} + \frac{1}{\rho} (\hat{\sigma}_d : \hat{D} - \frac{1}{T} \bar{q} \cdot \bar{\nabla} T) \geq 0. \quad (22)$$

where ρ is mass density, \bar{q} is the heat flux vector, $\hat{\sigma}_d$ is the deviatoric component of the Cauchy stress tensor $\hat{\sigma}$, Ψ is the free (Helmholtz) energy, S is the entropy and Q is the entropy production per unit mass. We accept the following expression for the free energy:

$$\Psi = \Psi_0 + (c - S_0)(T - T_0) - cT \ln \frac{T}{T_0} + W, \quad (23)$$

where S_0 and Ψ_0 are the entropy and the free energy in the equilibrium stress-free state at the reference temperature T_0 and c is the specific heat. The second and third terms on the right-hand side of Eq. (23) characterize the energy of thermal motion. Unlike conventional theories of rubber elasticity³⁰, the terms associated with configurational entropy of chains

are disregarded in Eq. (23). According to Ref.³¹, this approximation is acceptable, provided that

$$\mu \gg k_B T N,$$

where k_B is Boltzmann's constant. In the sequel, we suppose that this inequality is satisfied.

Substituting Eqs. (14) and (23) into Eq. (22) and assuming changes in the concentration of junctions to be rather slow (which means that Eq. (21) for the derivative of the mechanical energy W with respect to time may be used), we arrive at the formula

$$T \frac{dQ}{dt} = \left(\frac{\hat{\sigma}_d}{\rho} - \hat{\Upsilon} \right) : \hat{D} - \left(S - S_0 - c \ln \frac{T}{T_0} \right) \frac{dT}{dt} + J - \frac{1}{\rho T} \bar{q} \cdot \bar{\nabla} T \geq 0. \quad (24)$$

Applying the conventional reasoning²⁹ to Eq. (24), we find that the expressions in braces vanish. This assertion results in the standard formula for the entropy

$$S = S_0 + c \ln \frac{T}{T_0}, \quad (25)$$

where the configurational entropy of the network is neglected, and, together with Eqs. (20) and (21), the constitutive equation

$$\hat{\sigma}(t) = -P(t) \hat{I} + G[1 + \nu(t)]^2 [\bar{\nabla}_0 \bar{r}(t)]^\top \cdot \int_0^{2\pi} d\varphi \int_0^\pi \frac{e(t, \vartheta, \varphi)}{1 - n(t, \vartheta, \varphi)} \frac{\bar{l} \otimes \bar{l}}{\bar{l} \cdot \hat{C}(t) \cdot \bar{l}} \sin \vartheta d\vartheta \cdot \bar{\nabla}_0 \bar{r}(t), \quad (26)$$

where $P(t)$ is pressure and $G = \rho \mu m \Xi_0^2 / (4\pi)$. We substitute Eqs. (25) and (26) into Eq. (24) and find that the rate of entropy production is nonnegative for an arbitrary loading program, provided that

1. the heat flux vector \bar{q} obeys the Fourier law $\bar{q} = -\kappa \bar{\nabla} T$ with a positive thermal diffusivity κ ,
2. the function $n(t, \vartheta, \varphi)$ satisfies the kinetic equation

$$\frac{\partial n}{\partial t}(t, \vartheta, \varphi) = \alpha(t) e(t, \vartheta, \varphi) \left\{ \frac{2\eta[1 - n(t, \vartheta, \varphi)]}{1 + \eta n(t, \vartheta, \varphi)} - e(t, \vartheta, \varphi) \right\}, \quad n(0, \vartheta, \varphi) = 0, \quad (27)$$

where α is a nonnegative function of time.

We postulate that the rate of trans–cis transformation is proportional to the average number of strands in a chain,

$$\alpha(t) = \alpha_1 N(t), \quad (28)$$

where $\alpha_1 > 0$ is a material constant. Equation (28) is explained by the fact that the force opposing transition of a bond from its flexed to extended conformation is driven by the action of neighboring bonds, whereas stresses in these bonds are inversely proportional to the number of strands in a chain, see Eq. (3). Combining Eqs. (27) and (28) and using Eqs. (10) and (12), we arrive at the nonlinear differential equation

$$\frac{\partial n}{\partial t}(t, \vartheta, \varphi) = \alpha_0 \frac{e(t, \vartheta, \varphi)}{1 + \nu(t)} \left\{ \frac{2\eta[1 - n(t, \vartheta, \varphi)]}{1 + \eta n(t, \vartheta, \varphi)} - e(t, \vartheta, \varphi) \right\}, \quad n(0, \vartheta, \varphi) = 0 \quad (29)$$

with $\alpha_0 = \alpha_1/(m\Xi_0)$.

5. Evolution of the concentration of junctions

To close the model, the kinetics of stress–induced changes in the concentration of temporary junctions should be described. Denote by M_0 the total concentration (per unit mass) of entanglements (both loose and tight). Adopting the first-order kinetics for the mechanically-induced evolution of the number of tight entanglements, we assume that the rate of increase in the concentration of active entanglements is proportional to the current number of loose ones,

$$\frac{dM}{dt}(t) = \beta_*(t)[M_0 - M(t)], \quad (30)$$

where $\beta_*(t)$ is a positive function. It follows from Eqs. (12) and (30) that

$$\frac{d\nu}{dt}(t) = \beta_*(t)[\nu_0 - \nu(t)], \quad (31)$$

where the quantity

$$\nu_0 = 2 \frac{M_0 - M(0)}{\Xi_0}$$

equals the ratio of the initial number of loose entanglements to the initial number of chains. We postulate that the rate of growth for the number of active entanglements, β_* , is proportional to the mechanical energy per chain and inversely proportional to the number of strands in a chain,

$$\beta_*(t) = \beta_0 \frac{w_0(t)}{N(t)}, \quad (32)$$

where $\beta_0 > 0$ is a material constant. The proportionality of β_* to the average mechanical energy, w_0 , reflects the fact that tightening of loose entanglements is driven by mechanical factors. In general, any measure of straining may be chosen instead of w_0 on the right-hand side of Eq. (31), see a discussion of this issue in^{13,15}. We introduce the strain energy density, w_0 , by analogy with conventional models for damage of elastomers³². The inverse proportionality of β_* to the average number of strands in a chain, N , reflects slowing down of the process of tightening entanglements with an increase in the average length of chains. The latter is driven by the growth of the chains' mobility (estimated in terms of the number of available configurations).

It follows from Eqs. (10), (12), (31) and (32) that the function $\nu(t)$ obeys the kinetic equation

$$\frac{d\nu}{dt}(t) = \frac{\beta}{4\pi} [\nu_0 - \nu(t)] \int_0^{2\pi} d\varphi \int_0^\pi \frac{e^2(t, \vartheta, \varphi)}{1 - n(t, \vartheta, \varphi)} \sin \vartheta d\vartheta, \quad \nu(0) = 0, \quad (33)$$

where $\beta = \beta_0 \mu / 2$. Governing equations (26), (29) and (33) are determined by 5 adjustable parameters: an analog of the shear modulus G , the rate of trans–cis transition α_0 , the rate of stress–induced increase in the concentration of active entanglements β , the constant η which characterizes the end-to-end elongation of a chain driven by transformation of a bond from its flexed to extended conformation, and the ratio, ν_0 , of the initial number of loose entanglements to the initial number of chains. To determine these quantities, we analyze uniaxial extension of a rod.

6. Uniaxial tension of a specimen

At uniaxial tension of an incompressible medium, Cartesian coordinates in the deformed state, x_i , are expressed in terms of the Cartesian coordinates in the stress-free state, X_i , by the formulas

$$x_1 = k(t)X_1, \quad x_2 = k^{-\frac{1}{2}}(t)X_2, \quad x_3 = k^{-\frac{1}{2}}(t)X_3,$$

where $k = k(t)$ is the extension ratio. It follows from these equalities and Eq. (6) that

$$\begin{aligned} \bar{\nabla}_0 \bar{r}(t) &= k(t)\bar{e}_1\bar{e}_1 + k^{-\frac{1}{2}}(t)(\bar{e}_2\bar{e}_2 + \bar{e}_3\bar{e}_3), \\ \hat{C}(t) &= k^2(t)\bar{e}_1\bar{e}_1 + k^{-1}(t)(\bar{e}_2\bar{e}_2 + \bar{e}_3\bar{e}_3). \end{aligned} \quad (34)$$

The unit vector \bar{l} is given by

$$\bar{l} = \cos \vartheta \bar{e}_1 + \sin \vartheta (\cos \varphi \bar{e}_2 + \sin \varphi \bar{e}_3), \quad (35)$$

which implies that the tensor $\bar{l} \otimes \bar{l}$ is determined by the matrix

$$\bar{l} \otimes \bar{l} = \begin{bmatrix} \cos^2 \vartheta & \sin \vartheta \cos \vartheta \cos \varphi & \sin \vartheta \cos \vartheta \sin \varphi \\ \sin \vartheta \cos \vartheta \cos \varphi & \sin^2 \vartheta \cos^2 \varphi & \sin^2 \vartheta \sin \varphi \cos \varphi \\ \sin \vartheta \cos \vartheta \sin \varphi & \sin^2 \vartheta \sin \varphi \cos \varphi & \sin^2 \vartheta \sin^2 \varphi \end{bmatrix}. \quad (36)$$

Equations (34) and (35) yield

$$\bar{l} \cdot \hat{C}(t) \cdot \bar{l} = k^2(t) \cos^2 \vartheta + k^{-1}(t) \sin^2 \vartheta. \quad (37)$$

Because of the axial symmetry of deformation, the functions $n = n(t, \vartheta)$ and $e = e(t, \vartheta)$ are independent of φ , which implies that all terms but $\bar{l} \otimes \bar{l}$ on the right-hand side of Eq. (26) are independent of φ . It follows from Eq. (36) that

$$\frac{1}{2\pi} \int_0^{2\pi} \bar{l} \otimes \bar{l} d\varphi = \cos^2 \vartheta \bar{e}_1\bar{e}_1 + \frac{1}{2} \sin^2 \vartheta (\bar{e}_2\bar{e}_2 + \bar{e}_3\bar{e}_3).$$

Substitution of this expression and Eqs. (34) and (35) into Eq. (26) implies that

$$\hat{\sigma}(t) = \sigma(t)\bar{e}_1\bar{e}_1 + \sigma_0(t)(\bar{e}_2\bar{e}_2 + \bar{e}_3\bar{e}_3),$$

where

$$\begin{aligned}\sigma(t) &= -P(t) + 2\pi G[1 + \nu(t)]^2 \int_0^\pi \frac{k^2(t) \cos^2 \vartheta}{k^2(t) \cos^2 \vartheta + k^{-1}(t) \sin^2 \vartheta} \frac{e(t, \vartheta)}{1 - n(t, \vartheta)} \sin \vartheta d\vartheta, \\ \sigma_0(t) &= -P(t) + \pi G[1 + \nu(t)]^2 \int_0^\pi \frac{k^{-1}(t) \sin^2 \vartheta}{k^2(t) \cos^2 \vartheta + k^{-1}(t) \sin^2 \vartheta} \frac{e(t, \vartheta)}{1 - n(t, \vartheta)} \sin \vartheta d\vartheta.\end{aligned}\quad (38)$$

The boundary condition on the lateral surface of the specimen implies that $\sigma_0(t) = 0$.

Combining this equality with Eq. (38), we find the longitudinal stress

$$\sigma(t) = \pi G[1 + \nu(t)]^2 \int_0^\pi \frac{2k^2(t) \cos^2 \vartheta - k^{-1}(t) \sin^2 \vartheta}{k^2(t) \cos^2 \vartheta + k^{-1}(t) \sin^2 \vartheta} \frac{e(t, \vartheta)}{1 - n(t, \vartheta)} \sin \vartheta d\vartheta.$$

Introducing the notation

$$z = \cos \vartheta, \quad \tilde{e}(t, z) = e(t, \vartheta), \quad \tilde{n}(t, z) = n(t, \vartheta)$$

and bearing in mind that \tilde{e} and \tilde{n} are even functions of z , we obtain

$$\sigma(t) = E[1 + \nu(t)]^2 \int_0^1 \frac{2k^2(t)z^2 - k^{-1}(t)(1 - z^2)}{k^2(t)z^2 + k^{-1}(t)(1 - z^2)} \frac{\tilde{e}(t, z)}{1 - \tilde{n}(t, z)} dz, \quad (39)$$

where

$$E = \frac{1}{2} \rho \mu m \Xi_0^2. \quad (40)$$

It follows from Eqs. (8), (34) and (35) that

$$\tilde{e}(t, z) = \ln \frac{[k^2(t)z^2 + k^{-1}(t)(1 - z^2)]^{\frac{1}{2}}}{1 + \eta \tilde{n}(t, z)}. \quad (41)$$

In the sequel, we focus on stretching with a constant rate of engineering strain, $\dot{\epsilon}_0 > 0$,

$$k(t) = 1 + \dot{\epsilon}_0 t. \quad (42)$$

Combining Eqs. (29) and (42), we arrive at the kinetic equation

$$\frac{\partial \tilde{n}}{\partial k} = a \left[\frac{2\eta(1 - \tilde{n})}{1 + \eta \tilde{n}} - \tilde{e} \right] \tilde{e}, \quad \tilde{n}(1, z) = 0 \quad (43)$$

where $a = \alpha/\dot{\epsilon}_0$. Substituting expression (42) into Eq. (33) and calculating the integral over φ , we find that

$$\frac{d\nu}{dk} = b(\nu_0 - \nu) \int_0^1 \frac{\tilde{e}^2 dz}{1 - \tilde{n}}, \quad \nu(1) = 0, \quad (44)$$

where $b = \beta/\dot{\epsilon}_0$. Equations (39), (41), (43) and (44) are determined by 5 adjustable parameters: E , a , b , η and ν_0 . This number is quite comparable with the number of experimental constants employed in conventional stress-strain relations in finite elasticity of elastomers^{2,4,14,33}.

7. Comparison with experimental data

To determine adjustable parameters, we fit observations for natural rubber vulcanizates in uniaxial tensile tests with the strain rate $\dot{\epsilon}_0 = 2.0 \text{ min}^{-1}$ at room temperature. For a description of specimens and the experimental procedure, see Refs.^{19,20}.

We begin by matching experimental data in cyclic tests with the maximal elongation $k_{\max} = 6.0$ for a vulcanize with an unspecified composition. First, we approximate the stress-strain curve for a virgin sample. Given a Young's modulus, E , the constants a , b , η and ν_0 are found by the steepest-descent algorithm. The parameter E is determined by the least-squares technique. Afterwards, we fix the values b and ν_0 (which are responsible for the evolution of the concentration of junctions) and match stress-strain curves measured after retraction by using only three constants: E , a and η . Experimental data in tests with various numbers of cycles, i , are depicted in Figure 1 together with results of numerical simulation. Material constants are listed in Table 1. The parameters E , a and η are plotted versus the number of cycles i in Figures 2 and 3, which show that observations are fairly well approximated by the stretched exponential functions

$$E = E_0 \cdot 10^{i^{\kappa_E}}, \quad a = a_0 \cdot 10^{i^{\kappa_a}}, \quad \eta = \eta_0 \cdot 10^{i^{\kappa_\eta}}, \quad (45)$$

where the constants E_0 , a_0 , η_0 and κ_E , κ_a , κ_η are found by the least-squares algorithm.

We proceed by fitting observations for a natural rubber vulcanize with an unspecified composition in tensile loading-unloading tests with an increasing maximal amplitude of stretching, k_{\max} . First, we approximate experimental data for a virgin specimen and de-

termine adjustable parameters using the steepest-descent procedure. Afterwards, we fix the constants b and ν_0 and match stress-strain curves measured after retraction with the help of three adjustable parameters: E , a and η . Figure 4 demonstrates good agreement between experimental data and results of numerical simulation with adjustable parameters collected in Table 2. The quantities E , a and η are plotted in Figures 5 to 7 versus the number of cycles i . These figures reveal an acceptable quality of fitting experimental data by Eq. (45).

To evaluate the influence of annealing (24 h at the temperature $T = 100$ °C) on adjustable parameters in the constitutive equations, we approximate observations in tensile tests for three vulcanizates: A (polysulfide crosslinks), B (monosulfide crosslinks) and C (carbon–carbon crosslinks) with various amounts of crosslinkers (sulfur and dicumyl peroxide, respectively). A detailed description of the composition of specimens is presented in¹⁹. For any type of vulcanizates, we begin by fitting the stress–strain curve for a virgin sample with the minimum content of crosslinker, ϕ , and find experimental constants by using the steepest-descent algorithm. Afterwards, we fix the quantities b and ν_0 and match other observations by using only 3 adjustable parameters: E , a and η . Experimental data together with results of numerical simulation are depicted in Figures 8 to 10 for vulcanize A, in Figures 11 to 13 for vulcanize B and in Figures 14 and 15 for vulcanize C. Experimental constants are collected in Tables 3 to 5.

To compare the effects of thermal recovery and recovery by swelling, we match experimental data in tensile tests for a virgin specimen and for the same specimen after retraction (vulcanizates A, B and C with unspecified compositions), and repeat the same procedure for a recovered sample (swollen in benzene for 24 h and dried in vacuum). Adjustable parameters are found by using the same numerical procedure as for the specimens annealed at an elevated temperature. Observations and results of numerical simulation are depicted in Figures 16 to 18, whereas material constants are listed in Table 6.

8. Discussion

Figures 1, 4, 8 to 18 demonstrate fair agreement between experimental data and results of numerical analysis, which implies that the model may be applied to fit observations in uniaxial tensile tests with the axial elongation up to $k_{\max} = 8.0$.

Figures 3 and 7 show that the parameter η increases with the number of cycles, i . This conclusion is also confirmed by the data listed in Tables 3 to 6 (results for the first and second stretching). On the contrary, recovery of specimens (by annealing at an elevated temperature and by swelling) reduces η . This means that the quantity η may be treated as a parameter responsible for material damage at the micro-level. Because η reflects the average end-to-end elongation of a chain driven by an individual trans-cis transition (which implies that it may be thought of as an average measure of coiling of a chain), an increase in η under cyclic stretching is tantamount to an increase in the average size of a globule formed by a chain. This picture results in the conclusion that recovery of natural rubber vulcanizates may be treated as coiling of long chains. Tables 3 to 5 evidence that this process occurs more intensively for rubbery polymers with high concentrations of crosslinkers, and vulcanizates with dicumyl peroxide are annealed more effectively than those with sulfide crosslinks. These tables also show that the parameter η monotonically decreases with the growth of the content of crosslinker, ϕ . Because the growth of the concentration of chemical crosslinks results in an increase in the volume fraction of junctions (which is confirmed by the growth of Young's modulus with ϕ), and, as a consequence, a decrease in the average length of a chain, N , we may conclude that short chains are coiled up relatively more strongly [the qualification "relatively" is important here, because η is multiplied by the number of strands in a chain, N , in Eq. (7)] than longer ones.

Tables 3 to 6 show that at the second stretching the rate of transition from the flexed to extended conformation of bonds, a , exceeds that for a virgin specimen (the data for vulcanizate B in Table 6 are the only exception from this rule). This observation may also be treated as some kind of material damage: if we take a bond as a hinge, then straightening

two rods linked by the hinge occurs more easily for a preloaded sample than for a virgin one. Tables 3 to 5 reveal that a substantially grows with the concentration of crosslinker, ϕ . This increase may be associated with appropriate changes in η : an increase in the degree of coiling makes trans–cis transitions easier. In most cases, annealing of specimens (thermal and by swelling) results in a decrease in a which is accompanied by a decrease in η . However, for vulcanize A with high concentrations of crosslinker, an inverse tendency is observed: despite a decrease in η , the rate of transition from the flexed to extended conformation increases, see Tables 3 and 6.

Young's modulus E strongly increases with the content of crosslinker. This conclusion is in accord with Eq. (40) which implies that E is proportional to the square of the initial number of chains. Tables 3 to 6 demonstrate that the elastic modulus for a recovered specimen exceeds that for a prestrained material. The growth of E during recovery seems quite natural, provided that the recovery process is associated with an increase in the concentration of entanglements.

Unlike experimental data collected in Table 2, Table 1 demonstrates that cyclic loading results in a pronounced decrease in a and E with the number of cycles, i . Figure 2 reveals that this decrease may be fairly well approximated by the stretched exponential law. To explain the difference between the data listed in Tables 1 and 2, we refer to Figures 5 to 7, which evidence that E and a decrease with i at small amplitudes of stretching and strongly increase at large amplitudes. Changes in adjustable parameters observed in the cyclic test with an increasing amplitude are similar to those presented in Table 1 during the first 4 cycles and are analogous to those presented in Tables 3 to 5 when the maximum amplitude of stretching, k_{\max} , exceeds 4. One can only speculate about a physical mechanism for this phenomenon. As a possible explanation, we suppose that cyclic loading affects the internal structure of a rubber vulcanize in different ways at small and large amplitudes of stretching. Periodic loading with amplitudes which do not exceed some threshold results in material training similar to that occurring at isothermal annealing (Table 1). On the contrary, cyclic stretching with amplitudes exceeding the threshold strain results in damage

of the internal structure which is reflected by the data collected in Tables 2 to 5.

For each series of tests, the parameters b and ν_0 are found from the condition of the best fit for one stress-strain curve and remain fixed in matching observations for other curves. Excellent agreement between results of numerical simulation and experimental data leads to the conclusion that these parameters are not affected by mechanical factors.

Table 6 reveals that the differences between the parameters a and E found by fitting observations on recovered specimens at the first and second stretching are rather small compared with those for virgin samples. This means that recovery by swelling is equivalent to equilibration of rubbery polymers. On the contrary, analogous differences in η remain practically constant, which confirms the main hypothesis of this study that stress-softening of elastomers may be associated with uncoiling of long chains.

9. Conclusions

Constitutive equations have been derived for the isothermal mechanical response of elastomers at finite strains. Stress-strain relations are developed using the laws of thermodynamics and are applied to fit experimental data in uniaxial tensile tests for several natural rubber vulcanizates. Fair agreement is demonstrated between experimental data and results of numerical simulation.

We study the effects of cyclic loading, annealing at elevated temperature and recovery by swelling on material constants. The following conclusions are drawn:

1. Stress-softening of elastomers is reflected by changes in the parameter η which characterizes a mechanically-induced increase in the average size of globules formed by long chains. The quantity η is increased under periodic stretching with large amplitudes (uncoiling of chains) and is decreased at recovery (by annealing or swelling).
2. In contrast to conventional models for stress-softening of rubbery polymers, fitting of observations demonstrates that Young's modulus is altered relatively weakly. This

implies that damage should be associated rather with changes in the topology of a temporary network than with rupture of long chains.

3. Cyclic straining results in a noticeable increase in the rate of trans–cis transition of bonds, a , with the number of cycles, i (which is fairly well described by the stretched exponential law). On the contrary, recovery of specimens (by thermal annealing and swelling) induces a decrease in a .
4. Young’s modulus, E , and the rate of transformation of bonds from their flexed to extended conformation, a , substantially increase with the content of crosslinker, ϕ , whereas the parameter η is a decreasing function of ϕ .
5. Adjustable parameters change in a similar way during thermal annealing of specimens at an elevated temperature and during recovery by swelling.
6. Cyclic loadings with relatively small and large amplitudes affect the internal structure of elastomers in different ways. Periodic straining with large amplitudes causes damage to the internal structure, whereas the influence of that with small amplitudes is tantamount to recovery of vulcanizate and may be thought of as a kind of training of rubbery polymers.
7. The material parameters b and ν_0 which reflect the kinetics of mechanically-induced transition of loose entanglements into the active state are rather robust. They weakly depend on the intensity of loading, as well as on the composition of vulcanizates and on the content of crosslinkers.
8. Recovery by swelling reduces the increments of Young’s modulus and the rate of trans–cis transition driven by a cycle of loading. This implies that swelling of a rubber vulcanizate induces equilibration of its mechanical properties.

The above assertions are obtained in the framework of the phenomenological model, which implies that they should be treated with caution. These conclusions may, however, be

taken as rather plausible assumptions (mechanically-induced uncoiling of chains, training of an elastomer by sub-threshold periodic stretching, acceleration of trans–cis transformations under loading, disentanglement at retraction, etc.) which have to be checked experimentally. Validation of these hypotheses will be the subject of a subsequent study.

Acknowledgement

ADD acknowledges financial support by the Israeli Ministry of Science through grant 1202–1–00.

REFERENCES

1. Govindjee S, Simo JC. *J Mech Phys Solids* 1991; 39: 87.
2. Arruda EM, Boyce MC. *J Mech Phys Solids* 1993; 41: 389.
3. Johnson MA, Beatty MF. *Continuum Mech Thermodyn* 1993; 5: 301.
4. Wu PD, van der Gessen E. *J Mech Phys Solids* 1993; 41: 427.
5. van der Bogert PAJ, de Borst R. *Arch Appl Mech* 1994; 64: 136.
6. Johnson MA, Beatty MF. *Int J Engng Sci* 1995; 33: 223.
7. Holzapfel GA, Simo JC. *Int J Solids Structures* 1996; 33: 3019.
8. Lion A. *Continuum Mech Thermodyn* 1996; 8: 153.
9. Bergstöm JS, Boyce MC. *J Mech Phys Solids* 1998; 46: 931.
10. Septanika EG, Ernst LJ. *Mech Mater* 1998; 30: 253, 265.
11. Ogden RW, Roxburgh DH. *Proc Roy Soc Lond A* 1999; 455: 2861.
12. Boyce MC, Arruda EM. *Rubber Chem Technol* 2000; 73: 504.
13. Beatty MF, Krishnaswamy S. *J Mech Phys Solids* 2000; 48: 1931.
14. Meissner B, Matějka L. *Polymer* 2000; 41: 7749, 2001; 42: 1143.
15. Mieche C, Keck J. *J Mech Phys Solids* 2000; 48: 323.
16. Mullins L. *J Rubber Res* 1947; 16: 275.
17. Mullins L, Tobin NR. *J Appl Polym Sci* 1965; 9: 2993.
18. Harwood JAC, Mullins L, Payne AR. *J Appl Polym Sci* 1965; 9: 3011.
19. Harwood JAC, Payne AR. *J Appl Polym Sci* 1966; 10: 315, 1203.
20. Harwood JAC, Payne AR. *J Appl Polym Sci* 1967; 11: 1825.

21. Ernst LJ, Septanika EG. In: Dorfmann A, Muhr A., eds. Constitutive models for rubber, Rotterdam: Balkema, 1999, p. 169.
22. Roland CM. Rubber Chem Technol 1989; 62: 863, 880.
23. Boue F, Edwards SF, Vilgis TA. J Phys France 1988; 49: 1635.
24. Bensimon D, Dohmi D, Mezard M. Europhys Lett 1998; 42: 97.
25. Robertson RE. J Chem Phys 1966; 44: 3950.
26. Everaers R. Eur Phys J B 1998; 4: 341.
27. Drozdov AD. Acta Mech 2000; 139: 171.
28. Kar KK, Bhowmick AK. J Appl Polym Sci 1997; 64: 1541.
29. Coleman BD, Gurtin ME. J Chem Phys 1967; 47: 597.
30. Treloar LRG. The physics of rubber elasticity, Oxford: Clarendon Press, 1975.
31. Jones JL, Marques CM. J Phys France 1990; 51: 1113.
32. Miehe C. Eur J Mech A/Solids 1995; 14: 697.
33. Ball RC, Doi M, Edwards SF, Warner M. Polymer 1981; 22: 1010.

Figure legends

Figure 1: The true stress σ MPa versus the engineering strain ϵ for natural rubber with an unspecified composition. Circles: experimental data¹⁹. Solid lines: results of numerical simulation. Curve 1: $i = 1$; curve 2: $i = 2$; curve 3: $i = 3$; curve 4: $i = 8$

Figure 2: Young's modulus E MPa (unfilled circles) and the dimensionless parameter a (filled circles) versus the number of cycles i . Symbols: treatment of observations¹⁹. Solid lines: approximation of the experimental data by Eq. (45). Curve 1: $E_0 = 12.3705$, $\kappa_E = -0.0716$; curve 2: $a_0 = 9.2561$, $\kappa_a = -0.1219$

Figure 3: The dimensionless parameter η versus the number of cycles i . Circles: treatment of observations¹⁹. Solid lines: approximation of the experimental data by Eq. (45) with $\eta_0 = 4.1975$ and $\kappa_\eta = -0.2055$

Figure 4: The true stress σ MPa versus the engineering strain ϵ for natural rubber vulcanizate with an unknown composition. Circles: experimental data²⁰. Solid lines: results of numerical simulation. Curve 1: a virgin specimen; curve 2: the 4th stretching; curve 3: the 5th stretching; curve 4: the 6th stretching; curve 5: the 7th stretching; curve 6: the 8th stretching; curve 7: the 9th stretching

Figure 5: Young's modulus E MPa versus the number of cycles i . Circles: treatment of observations²⁰. Solid lines: approximation of the experimental data by Eq. (45). Curve 1: $E_0 = 21.5638$, $\kappa_E = -0.0125$; curve 2: $E_0 = 3.3807$, $\kappa_E = 0.5003$

Figure 6: The dimensionless parameter a versus the number of cycles i . Circles: treatment of observations²⁰. Solid lines: approximation of the experimental data by Eq. (45). Curve 1: $a_0 = 9.9095$, $\kappa_a = 0.0863$; curve 2: $a_0 = 3.7108$, $\kappa_a = 0.3952$

Figure 7: The dimensionless parameter η versus the number of cycles i . Circles: treatment of observations²⁰. Solid lines: approximation of the experimental data by Eq. (45). Curve 1: $\eta_0 = 4.6700$, $\kappa_\eta = -0.0035$; curve 2: $\eta_0 = 2.7620$, $\kappa_\eta = 0.2524$

Figure 8: The true stress σ MPa versus the engineering strain ϵ for natural rubber vulcanizate A ($\phi = 1.25$ phr). Circles: experimental data¹⁹. Solid lines: results of numerical

simulation. Curve 1: the first stretching; curve 2: the second stretching; curve 3: stretching after annealing

Figure 9: The true stress σ MPa versus the engineering strain ϵ for natural rubber vulcanizate A ($\phi = 2.50$ phr). Circles: experimental data¹⁹. Solid lines: results of numerical simulation. Curve 1: the first stretching; curve 2: the second stretching; curve 3: stretching after annealing

Figure 10: The true stress σ MPa versus the engineering strain ϵ for natural rubber vulcanizate A ($\phi = 4.17$ phr). Circles: experimental data¹⁹. Solid lines: results of numerical simulation. Curve 1: the first stretching; curve 2: the second stretching; curve 3: stretching after annealing

Figure 11: The true stress σ MPa versus the engineering strain ϵ for natural rubber vulcanizate B ($\phi = 0.2$ phr). Circles: experimental data¹⁹. Solid lines: results of numerical simulation. Curve 1: the first stretching; curve 2: the second stretching; curve 3: stretching after annealing

Figure 12: The true stress σ MPa versus the engineering strain ϵ for natural rubber vulcanizate B ($\phi = 0.4$ phr). Circles: experimental data¹⁹. Solid lines: results of numerical simulation. Curve 1: the first stretching; curve 2: the second stretching; curve 3: stretching after annealing

Figure 13: The true stress σ MPa versus the engineering strain ϵ for natural rubber vulcanizate B ($\phi = 0.6$ phr). Circles: experimental data¹⁹. Solid lines: results of numerical simulation. Curve 1: the first stretching; curve 2: the second stretching; curve 3: stretching after annealing

Figure 14: The true stress σ MPa versus the engineering strain ϵ for natural rubber vulcanizate C ($\phi = 0.5$ phr). Circles: experimental data¹⁹. Solid lines: results of numerical simulation. Curve 1: the first stretching; curve 2: the second stretching; curve 3: stretching after annealing

Figure 15: The true stress σ MPa versus the engineering strain ϵ for natural rubber vulcanizate C ($\phi = 3.5$ phr). Circles: experimental data¹⁹. Solid lines: results of numerical

simulation. Curve 1: the first stretching; curve 2: the second stretching; curve 3: stretching after annealing

Figure 16: The true stress σ MPa versus the engineering strain ϵ for natural rubber vulcanizate A with an unspecified composition. Circles: experimental data¹⁹. Solid lines: results of numerical simulation. Curve 1: a virgin sample, the first stretching; curve 2: a virgin sample, the second stretching; curve 3: a recovered sample, the first stretching; curve 4: a recovered sample, the second stretching

Figure 17: The true stress σ MPa versus the engineering strain ϵ for natural rubber vulcanizate B with an unspecified composition. Circles: experimental data¹⁹. Solid lines: results of numerical simulation. Curve 1: a virgin sample, the first stretching; curve 2: a virgin sample, the second stretching; curve 3: a recovered sample, the first stretching; curve 4: a recovered sample, the second stretching

Figure 18: The true stress σ MPa versus the engineering strain ϵ for natural rubber vulcanizate C with an unspecified composition. Circles: experimental data¹⁹. Solid lines: results of numerical simulation. Curve 1: a virgin sample, the first stretching; curve 2: a virgin sample, the second stretching; curve 3: a recovered sample, the first stretching; curve 4: a recovered sample, the second stretching

TABLES

Table 1. Adjustable parameters for NR vulcanizate

	a	η	E MPa	ν_0	b
1st stretching	8.9	4.12	12.48	1.7	0.6
2nd stretching	8.0	4.41	10.89	1.7	0.6
3rd stretching	7.8	4.50	10.13	1.7	0.6
8th stretching	5.5	4.57	8.79	1.7	0.6

Table 2. Adjustable parameters for NR vulcanizate

	a	η	E MPa	ν_0	b
1st stretching	9.9	4.67	21.65	1.7	0.35
4th stretching	7.9	4.36	14.69	1.7	0.35
5th stretching	14.1	4.63	19.52	1.7	0.35
6th stretching	14.4	4.93	20.85	1.7	0.35
7th stretching	17.0	5.19	23.61	1.7	0.35
8th stretching	19.2	5.53	29.64	1.7	0.35
9th stretching	23.2	5.95	41.66	1.7	0.35

Table 3. Adjustable parameters for vulcanizate A

	<i>a</i>	η	<i>E</i> MPa	ν_0	<i>b</i>
$\phi = 1.25$ phr					
1st stretching	13.5	4.27	12.66	1.6	0.4
2nd stretching	15.1	4.67	10.25	1.6	0.4
after annealing	15.0	4.47	11.41	1.6	0.4
$\phi = 2.50$ phr					
1st stretching	11.5	3.55	15.15	1.6	0.4
2nd stretching	14.4	4.11	15.15	1.6	0.4
after annealing	18.2	3.90	17.78	1.6	0.4
$\phi = 4.17$ phr					
1st stretching	12.3	3.21	22.24	1.6	0.4
2nd stretching	17.6	3.32	18.66	1.6	0.4
after annealing	18.4	3.32	21.06	1.6	0.4

Table 4. Adjustable parameters for vulcanizate B

	<i>a</i>	η	<i>E</i> MPa	ν_0	<i>b</i>
$\phi = 0.2$ phr					
1st stretching	10.9	4.60	13.43	1.7	0.2
2nd stretching	16.8	5.10	14.35	1.7	0.2
after annealing	16.4	4.81	16.04	1.7	0.2
$\phi = 0.4$ phr					
1st stretching	14.4	3.90	22.69	1.7	0.2
2nd stretching	24.7	4.20	24.26	1.7	0.2
after annealing	20.4	4.00	25.01	1.7	0.2
$\phi = 0.6$ phr					
1st stretching	20.4	3.66	34.84	1.7	0.2
2nd stretching	34.7	3.83	35.40	1.7	0.2
after annealing	33.0	3.62	39.12	1.7	0.2

Table 5. Adjustable parameters for vulcanizate C

	<i>a</i>	η	<i>E</i> MPa	ν_0	<i>b</i>
$\phi = 0.5$ phr					
1st stretching	8.4	5.61	8.37	1.7	0.3
2nd stretching	11.7	6.02	7.01	1.7	0.3
after annealing	11.1	5.65	8.65	1.7	0.3
$\phi = 3.5$ phr					
1st stretching	28.2	3.58	23.33	1.7	0.3
2nd stretching	38.1	3.67	22.34	1.7	0.3
after annealing	35.9	3.57	23.82	1.7	0.3

Table 6. Adjustable parameters for natural rubber vulcanizates

	<i>a</i>	η	<i>E</i> MPa	ν_0	<i>b</i>
Vulcanize A					
virgin samples					
1st stretching	10.9	4.40	23.48	1.6	0.4
2nd stretching	16.1	5.11	24.29	1.6	0.4
recovered samples					
1st stretching	16.7	5.01	24.11	1.6	0.4
2nd stretching	16.1	5.25	24.38	1.6	0.4
Vulcanize B					
virgin samples					
1st stretching	12.5	5.64	31.97	1.6	0.2
2nd stretching	9.5	6.04	23.52	1.6	0.2
recovered samples					
1st stretching	8.6	5.63	24.21	1.6	0.2
2nd stretching	10.5	5.91	23.62	1.6	0.2
Vulcanize C					
virgin samples					
1st stretching	7.8	5.62	25.34	1.6	0.2
2nd stretching	11.6	6.07	26.47	1.6	0.2
recovered samples					
1st stretching	9.6	5.66	27.21	1.6	0.2
2nd stretching	9.6	6.23	25.55	1.6	0.2

FIGURES

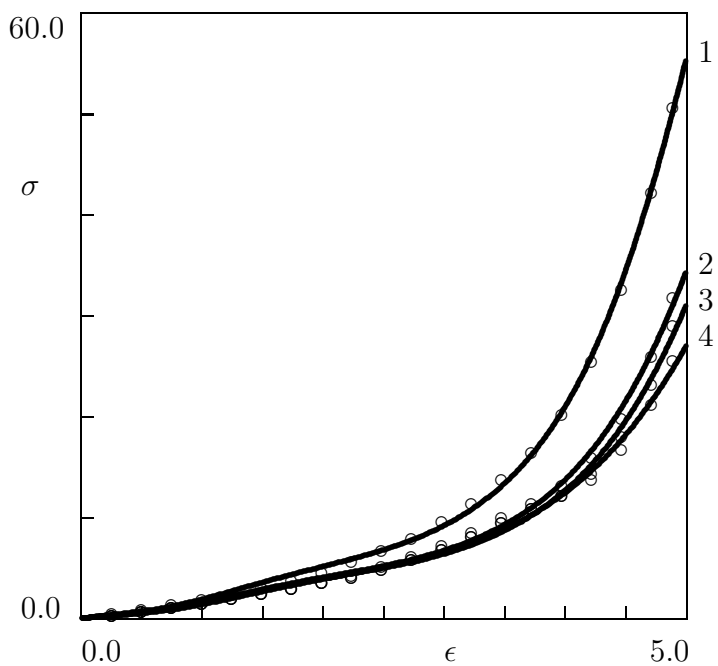


Fig. 1.

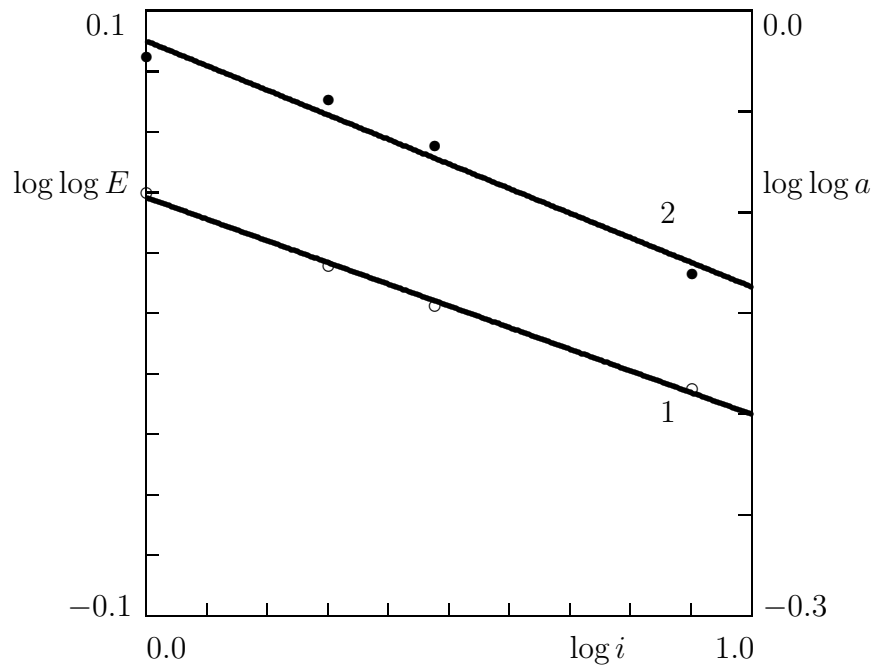


Fig. 2.

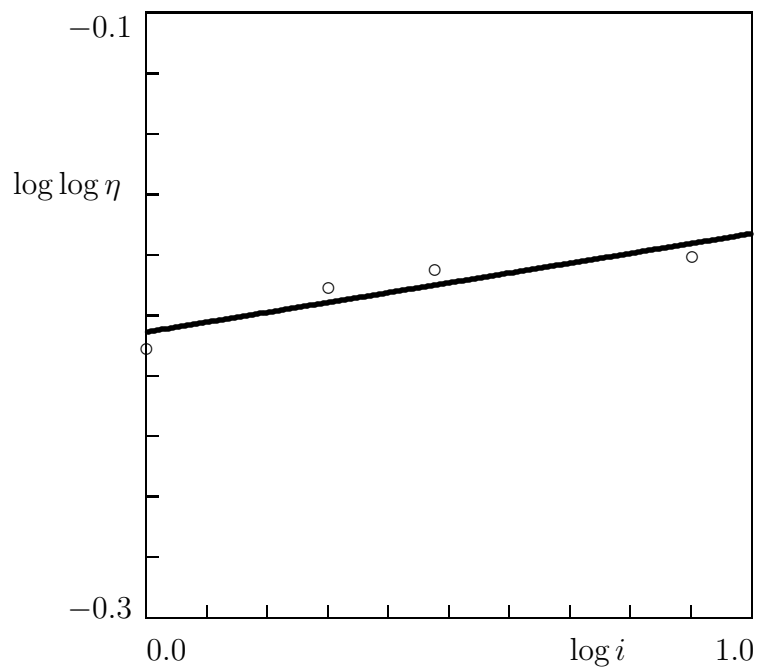


Fig. 3.

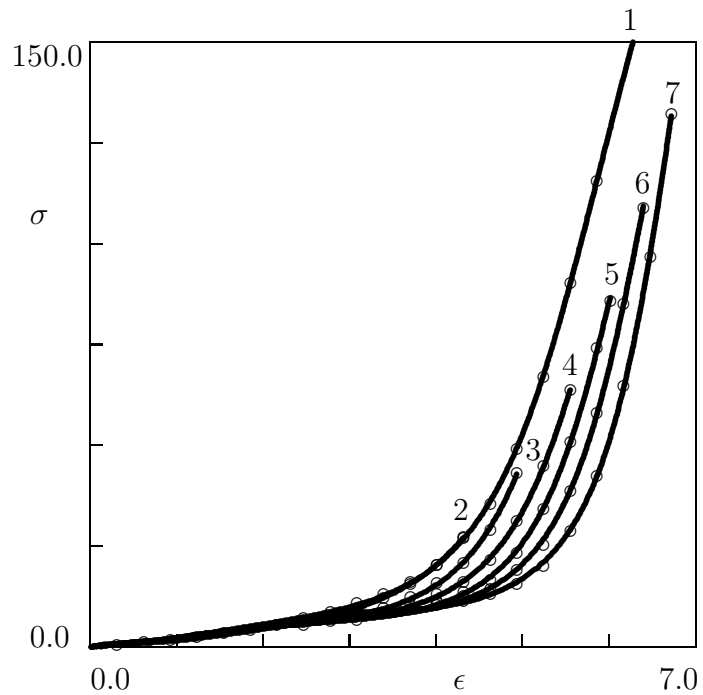


Fig. 4.

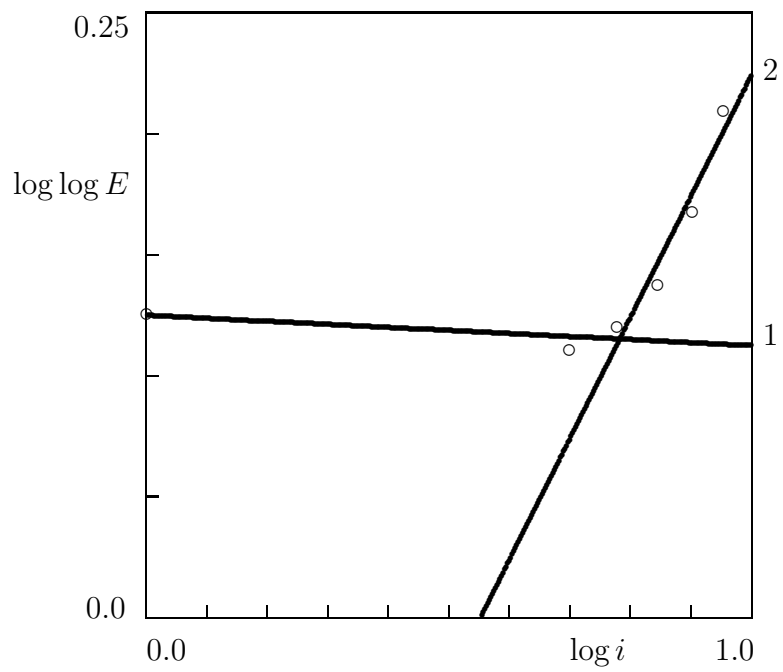


Fig. 5.

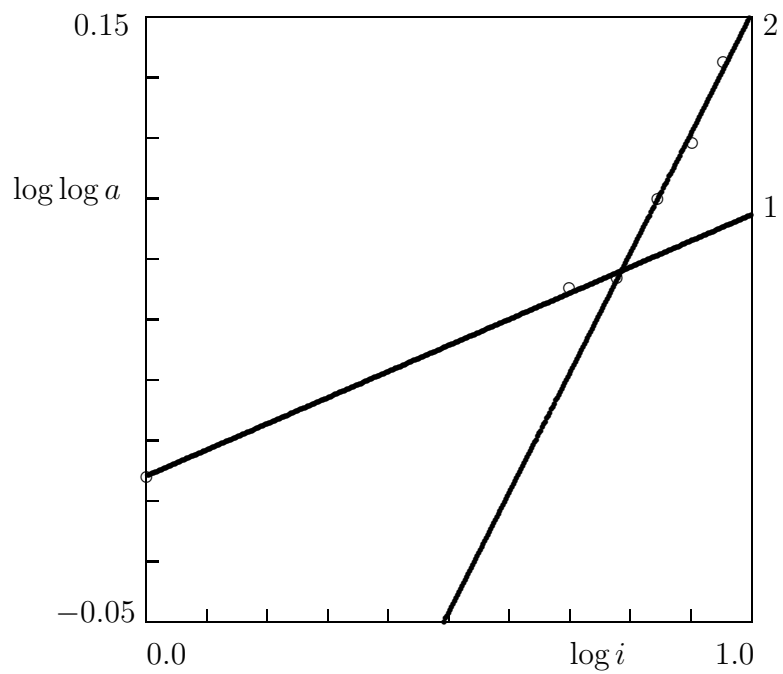


Fig. 6.

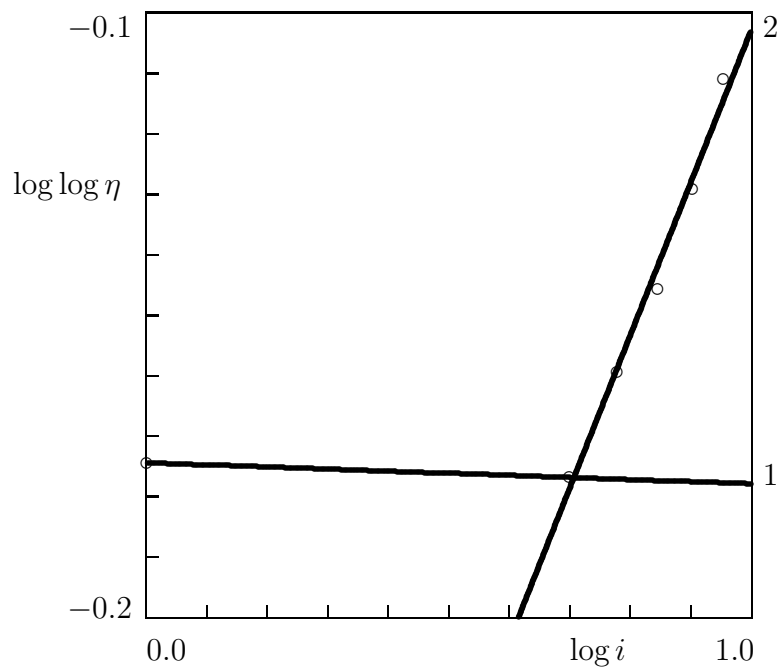


Fig. 7.

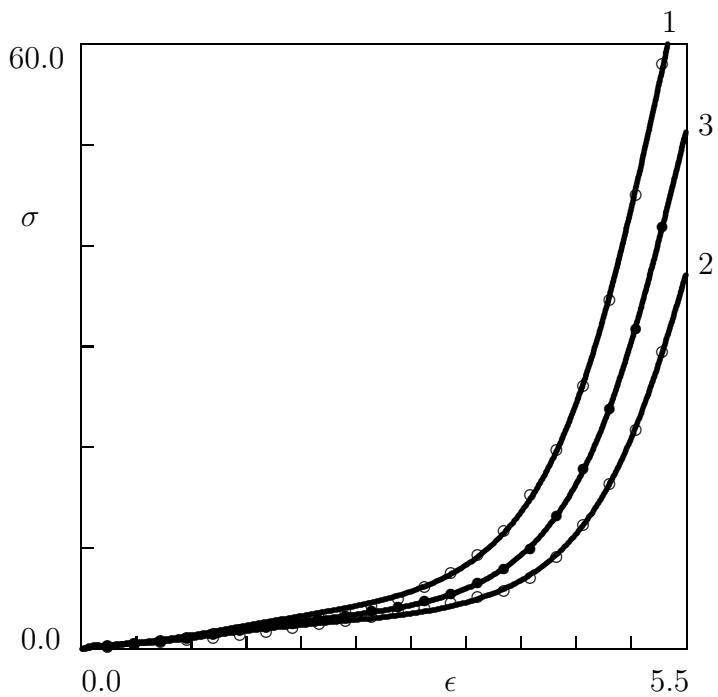


Fig. 8.

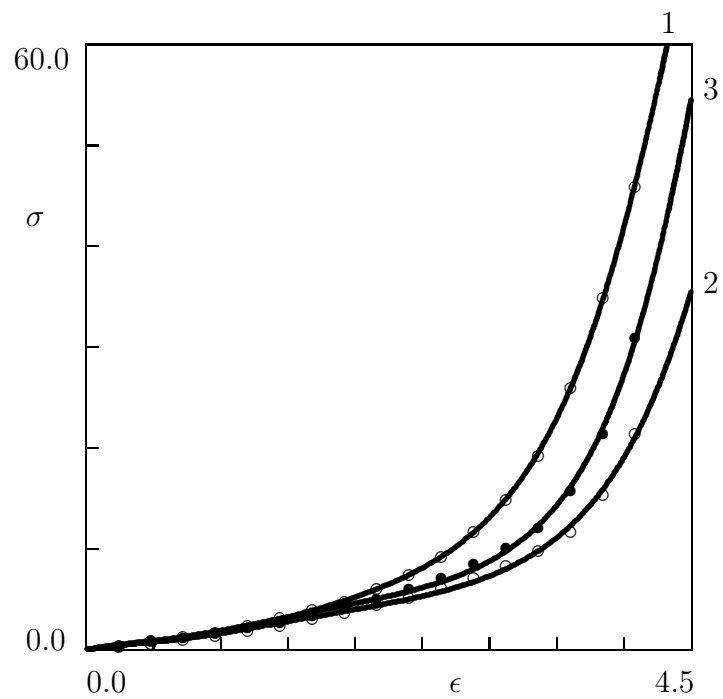


Fig. 9.

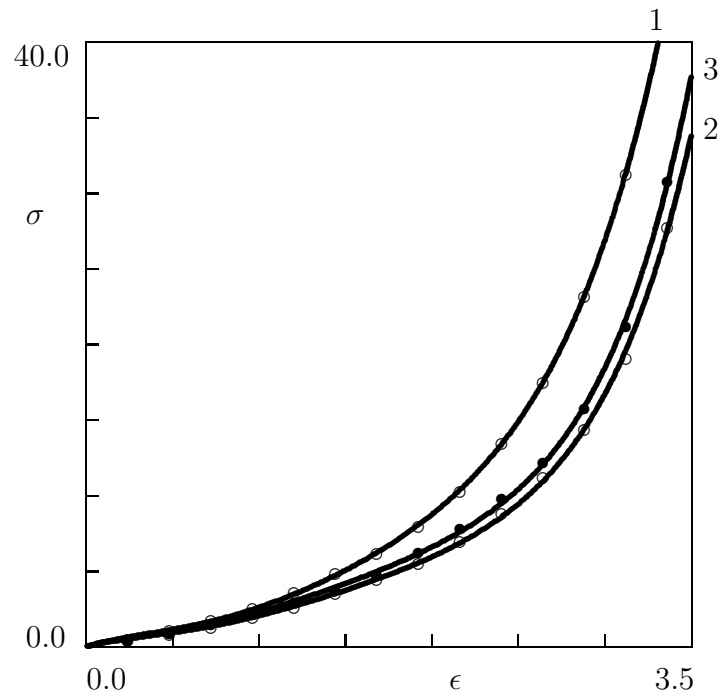


Fig. 10.

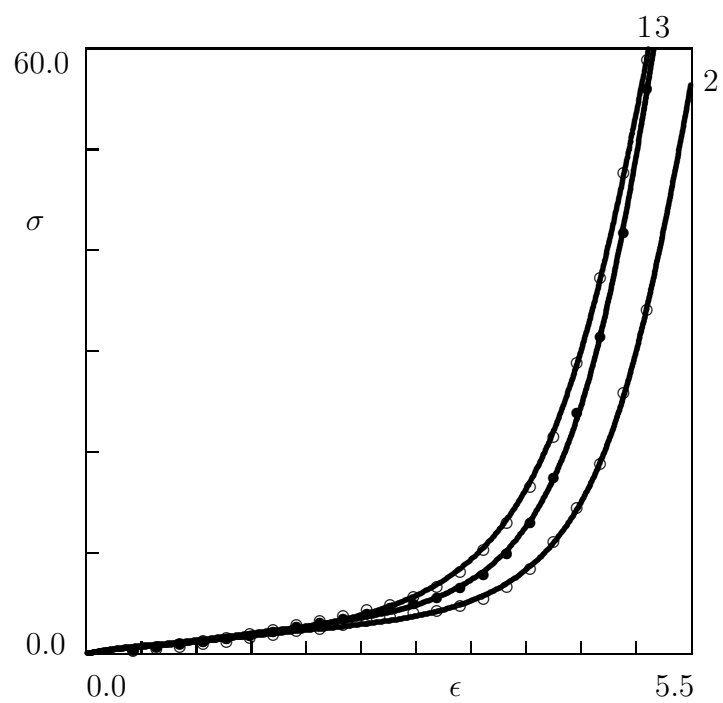


Fig. 11.

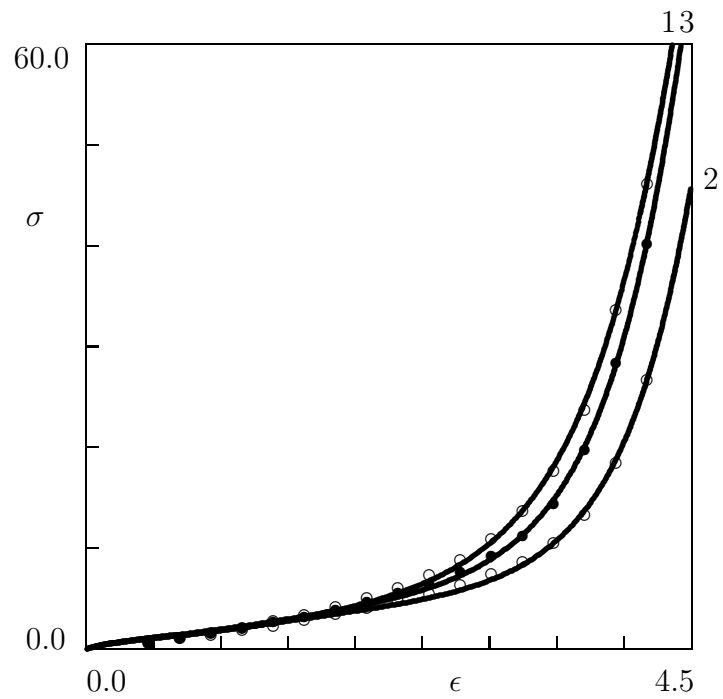


Fig. 12.

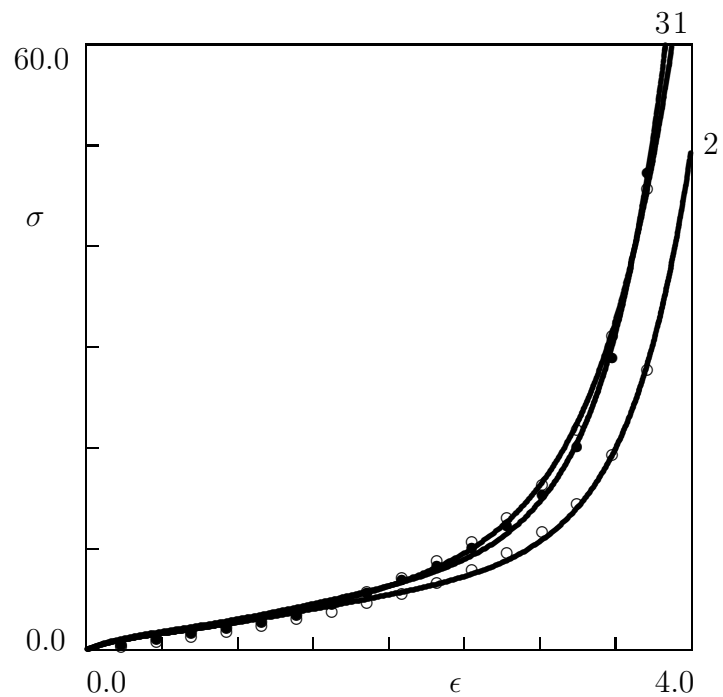


Fig. 13.

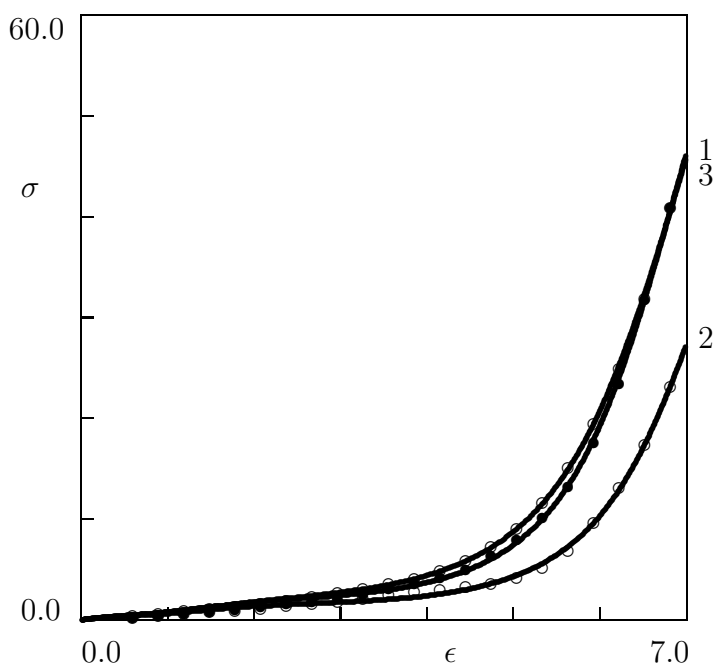


Fig. 14.

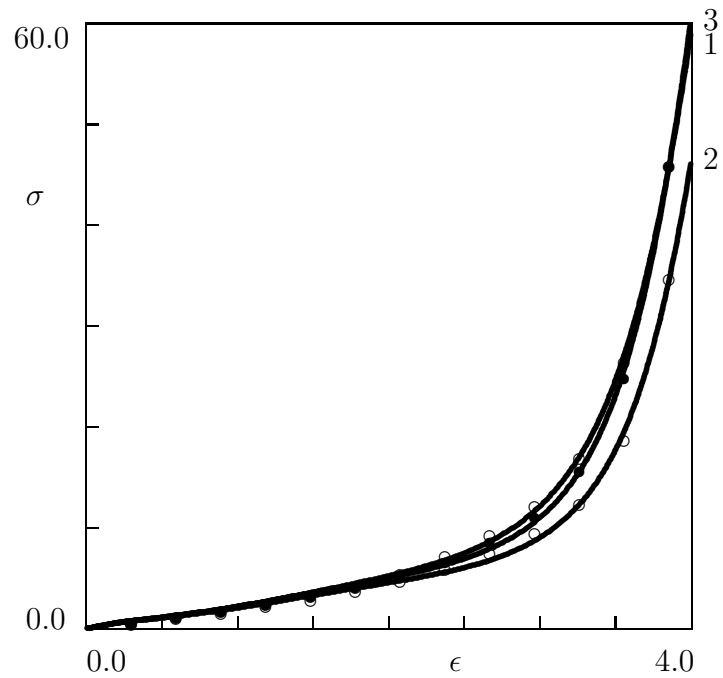


Fig. 15.

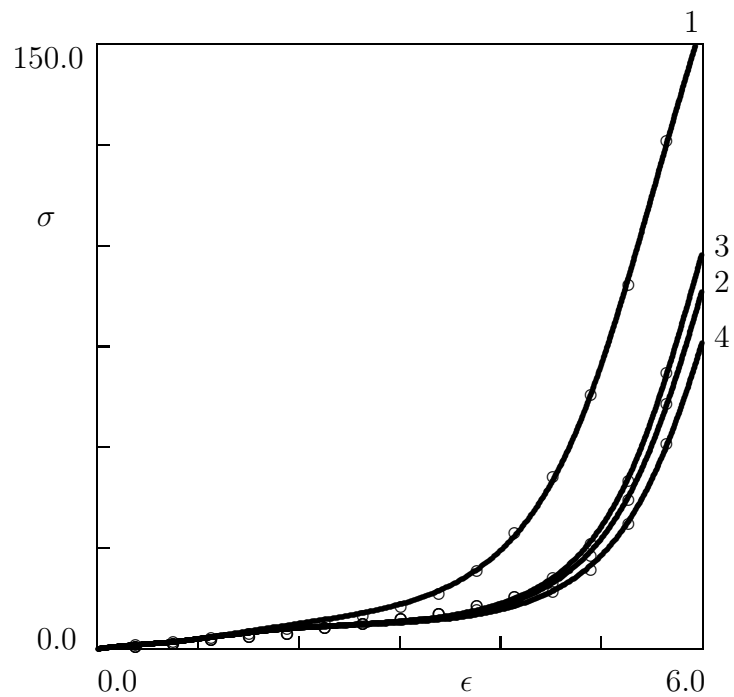


Fig. 16.

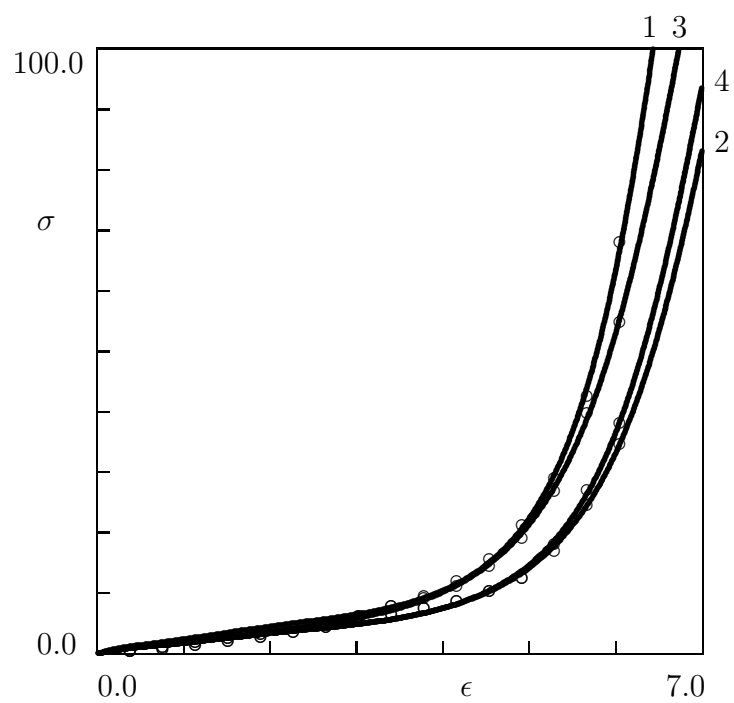


Fig. 17.

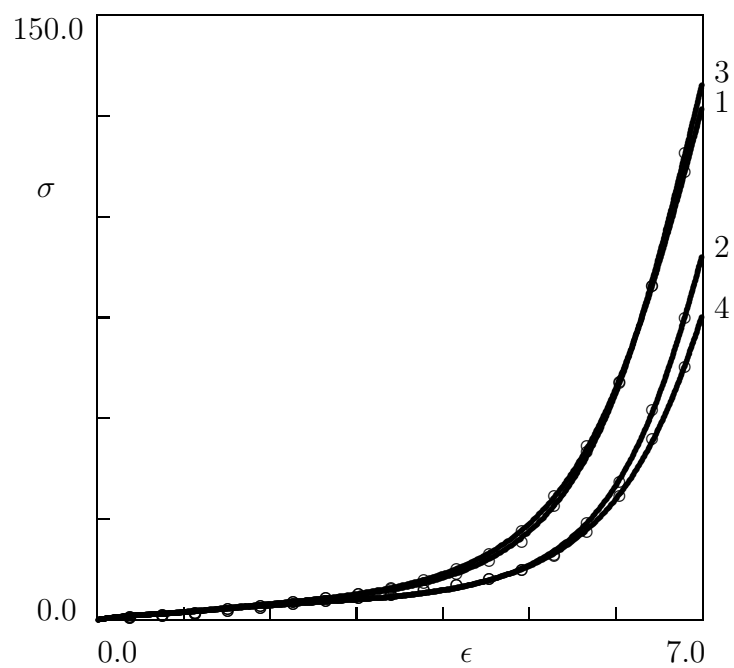


Fig. 18.